Available online at www.sciencedirect.com
ScienceDirect
Journal of Molecular Catalysis A: Chemical 281 (2008) 154–163
JOURNAL OF MOLECULAR CATALYSIS A: CHEMICAL
www.elsevier.com/locate/molcata

Al and Ti-containing mesoporous molecular sieves: Synthesis, characterization and redox activity in the anthracene oxidation

R.S. Araújo [a,1], D.C.S. Azevedo [a,*], E. Rodríguez-Castellón [b], A. Jiménez-López [b], C.L. Cavalcante Jr. [a]

[a] *Grupo de Pesquisas em Separações por Adsorção (GPSA), Department of Chemical Engineering – Universidade Federal do Ceará, Campus Universitário do Pici, Bl. 709, 60455-760 Fortaleza, CE, Brazil*
[b] *Department of Inorganic Chemistry, Crystallography and Mineralogy (Unidad Asociada al ICP-CSIC), Facultad de Ciencias, Universidad de Málaga, 29071 Málaga, Spain*

Available online 7 September 2007

Abstract

Mesoporous materials containing aluminum and titanium were obtained by direct synthesis at room temperature, using a sol–gel method with two reaction steps (acid and alkaline hydrolysis). After solvent extraction and calcination (823 K), three solids, H-MCM-41, Al-MCM-41(10) and Ti-MCM-41(30) were obtained, where the numbers in parenthesis denote the Si/metal molar ratio. A hexagonal mesoporous silica containing titanium, Ti-HMS(30), was also prepared, using *n*-dodecylamine as a template at pH 10. Characterization of samples was made by ICP-OES, ATR-FTIR, XRD, N_2 adsorption at 77 K, XPS and ammonia TPD. The results indicate that the samples have low crystallinity, surface areas of 500–750 m^2/g, high degree of isomorphic substitution and, in certain cases, higher acidity (Brönsted and Lewis) as compared to a commercial Y zeolite (Si/Al = 1.5). Catalytic studies of anthracene oxidation in liquid phase at 348 K, using *tert*-butylhydroperoxide as oxidant agent showed that the Ti-HMS(30) sample is much more prone to produce 9,10-anthraquinone (yield >90%) than the other mesoporous samples. This performance is directly related to parameters such as surface area, nature of the heteroatom introduced, Si/Ti molar ratio and strength and concentration of acid sites. The reaction kinetic experiments show a great dependency of specific reaction rates with temperature (in the range 320–348 K) and an activation energy value of 15.2 kcal/mol. A set of experiments performed under factorial design indicated that an optimal oxidant/aromatic ratio is 5.5 and the optimal amount of catalyst is about 44.3 mg. In general, our results confirm that the synthesized materials are promising catalysts (redox and acid) for petrochemical applications.

Keywords: Mesoporous materials; Titanosilicates; Aluminosilicates; Acid strength; Anthracene oxidation

1. Introduction

Porous inorganic solids of the M41S family were first synthesized by Beck et al. in 1992 [1]. Since then, they have shown to be promising materials for industrial applications in adsorption and catalysis. Among the members of this class of materials, those known as MCM-41 have been most widely studied, mainly because of its pseudo-crystalline and textural properties, such as the hexagonal arrangement of one-dimensional channels [2], mean pore diameters in the range of 20–100 Å and high surface areas (>1000 m^2/g). In general, the structural and textural characteristics of such molecular sieves are directly related to the synthesis conditions under which they are prepared [3–8]: the nature of the surfactant, pH, presence of electrolytes, temperature, solvents, aging/preparation time, etc. On the other hand, the incorporation of heteroatoms in the MCM-41 structure, transition metals or Al, promotes the appearance of active catalytic sites (both acid or redox), which may suit them for interesting applications in heterogeneous catalysis involving voluminous reactants. As a matter of fact, the conversion of these reactants and the use of oxidants other than H_2O_2, for example, are serious limiting factors against the use of commercial zeolites in several redox reactions, mainly due to intrinsic diffusional resistances and/or steric hindrances [9,10]. The incorporation of metals such as Al, Cu, V, Cr, Ti, Fe, Ni, Mn and Zr within the MCM-41 matrix has recently gained considerable interest. The iso and non-isomorphic substitutions usually enhance catalytic activity in

* Corresponding author. Tel.: +55 85 3287 4403; fax: +55 85 3366 9610.
E-mail address: diana@gpsa.ufc.br (D.C.S. Azevedo).
[1] Present address: CEFETCE – Centro Federal de Educação Tecnológica do Ceará, Av. 13 de Maio, 2081, Fortaleza, CE. CEP 60040-531, Brazil.

1381-1169/$ – see front matter © 2007 Elsevier B.V. All rights reserved.
doi:10.1016/j.molcata.2007.09.001

processes of commercial interest such as: hydrocarbon catalytic cracking [11,12], isomerization [13,14], hydrodesulphurization [15,16], oxidation reactions, hydroxylation and epoxidation of aromatics, olefins and phenols [17–22], etc. Recently, isomorphously substituted metal ion (V, Ti, Cr, Mn, Fe, Co, Ni, Cu, Zn) containing MCM-41 solids were found to be active for liquid phase oxidation of anthracene to 9,10-anthraquinone at 353 K using benzene as a solvent and *t*-butylhydroperoxide as oxidant [23]. The order of selectivity to the mentioned quinone was Cr > Mn > Co > Cu > Fe > V > Ni > Zn > Ti. The conversion of anthracene was 79.5% and the selectivity towards the quinone was 97.9% for the sample Cr-MCM-41 (0.46 wt% of Cr). Higher yields to 9,10-anthraquinone, up to 93%, were obtained with Cr impregnated samples with Cr contents between 1 and 5 wt%.

The present work describes the synthesis of the mesoporous molecular sieves Al-MCM-41, Ti-MCM-41 and Ti-HMS, that is, using non-toxic metals ions unlike Cr or V, with pore diameters smaller than 34 Å and suitable surface acidity to promote high conversions in the oxidation of anthracene. Experimental evidence showed that the different coordination states of the incorporated heteroatoms have a marked influence on the catalytic activity of the synthesized solids, leading to the formation of either the target product 9,10-anthraquinone (product of the addition reaction) or a mixture of hydroxylated products (products of the substitution reactions). Among other uses, 9,10-anthraquinone is an important intermediate for the production of several dyes of textile industry. It is also employed in the isomerization of vegetable oils, in nickel electro-deposition, seed and grain protection and in the production of stabilizing additives [24].

2. Experimental

2.1. Sample preparation

Mesoporous samples were prepared by the sol–gel method in two reaction steps (acid and alkaline hydrolysis), as proposed by Aguado et al. [25]. The typical experimental procedure consisted of dissolution of tetraethylorthosilicate (TEOS) and aluminum triisopropoxide (AlTIPO), for the aluminosilicates, or titanium tetraisopropoxide (TiTIPO), for the titanosilicates, in ethanol, under mild stirring, followed by the addition of *n*-dodecylammonium chloride (DDACl) hydro-alcoholic solution previously shaken at room temperature (298 K) for 10 min. The hydro-alcoholic surfactant solution was prepared by dissolving 5 g dodecylamine in 20 mL ethanol. The pH was adjusted to 2 with dropwise addition of HCl (30 wt%). The molar composition of the synthesis gel is summarized in Table 1 for each of the synthesized materials. Acid hydrolysis was carried out for about 90 min, under mild stirring. After stirring was ceased, pH was adjusted to 10 with aqueous ammonia (30 wt%) so as to favour the condensation of silicate groups (alkaline hydrolysis). Reaction thus proceeded for 75–90 min under vigorous stirring. Following the alkaline step, the synthesized material was allowed to age for 20 h at room temperature in its own synthesis liquor under static conditions. The pH was kept at 10 by adding HCl 30 wt%), as required. The solids were filtered, washed with deionised water and dried overnight at 378 K. Then, they underwent solvent extraction (ethanol/HNO_3 0.1 M) for 2–4 h, followed by calcination at 823 K (∼3 h). For the sake of comparison, a pure siliceous sample was also prepared, by omitting the Al or Ti sources. The synthesized samples were labeled as Al-MCM-41(10), Ti-MCM-41(30) and H-MCM-41.

An additional sample of Ti-HMS was also prepared by following a neutral templating pathway (S^0I^0) using dodecylamine (DDA) as the organic template. The synthesis was thoroughly conducted in alkaline medium at room temperature (298 K) and H_2O_2 30% (0.01 mol) was added to prevent Ti^{4+} ions from precipitating as TiO_2 [26]. The molar composition was identical to that used in the preparation of the Ti-MCM-41 sample, by means of an electrostatic pathway S^+I^-, with pH kept at 10 during the whole reaction.

2.2. Sample characterization

Elemental chemical composition was determined by ICP-OES in a Perkin-Elmer optima 4300 spectrometer. Calcined samples were previously dissolved and digested in a mixture of HF 10%/HCl–HNO_3 (1:3). XRD powder spectra were obtained in a Philips X'PERT MPD apparatus with Cu Kα (λ = 1.5418 Å) as the radiation source in the range of $0 < 2\theta < 10^\circ$. The textural parameters of the solids were calculated from N_2 adsorption/desorption isotherms measured at 77 K in an Autosorb-MP apparatus, from Quantachrome. Samples were previously degassed for 2 h at 623 K under vacuum. IR absorbance measurements were performed in a BIO-RAD FX3000 spectrophotometer with a reflectance device (ATR). X-ray photoelectron spectra (XPS) were recorded on a Physical Electronics PHI 5700 spectrometer with Mg radiation (1235.6 eV) and a multi-channel detector. Calculations were executed assuming the signal of adventitious carbon C (1 s), at 284.8 eV, as reference. A PHI-ACESS ESCA V6.0F software was used for data acquisition and handling. Samples were previously degassed for 12 h under high vacuum ($<1.3 \times 10^{-6}$ Pa). The modified Auger parameter of Al (α') was calculated using

Table 1
Molar composition of synthesis gels and respective Si/Al and Si/Ti ratios

Sample	Gel molar composition	Si/M ratio (M = Al or Ti)
H-MCM-41	1TEOS, 0.30 DDACl, 5.20 EtOH, 23 H_2O	∞
Al-MCM-41(10)	1TEOS, 0.10 Al, 0.30 DDACl, 5.20 EtOH, 23 H_2O	10
Ti-MCM-41(30)	1TEOS, 0.033 Ti, 0.30 DDACl, 5.20 EtOH, 23 H_2O	30
Ti-HMS(30)	1TEOS, 0.033 Ti, 0.30 DDA, 5.20 EtOH, 23 H_2O	30

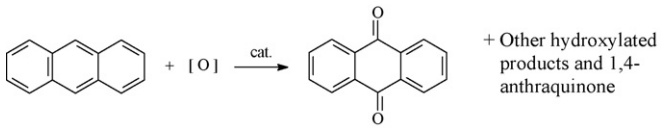

Fig. 1. Anthracene oxidation to 9,10-anthraquinone by peroxide reaction.

the following equation:

$$\alpha' = 1253.6 + \mathrm{KE}(\mathrm{Al_{KLL}}) - \mathrm{KE}(\mathrm{Al\,2p}) \quad (1)$$

where $\mathrm{KE}(\mathrm{Al_{KLL}})$ is the kinetic energy of the Auger electron of $\mathrm{Al_{KLL}}$ and KE(Al 2p), the kinetic energy of the photoelectron Al 2p.

Total surface acidity was assessed from temperature-programmed desorption (NH_3-TPD) of ammonia. Samples were heated at 823 K under N_2 flux in order to remove previously adsorbed impurities, followed by adsorption of ammonia at 373 K. The system was kept at this temperature for about 30 min, to ensure adsorption equilibrium (saturation) was reached. The base was then desorbed by increasing the temperature from 373 to 823 K at a rate of 10 K/min and ammonia concentration was detected on line in a Shimadzu GC-14A gas chromatograph using a thermal conductivity detector. The Lewis acidity of the samples was also investigated using pyridine as a probe molecule. IR spectra of the adsorbed pyridine (Py-FTIR) were recorded on a Schimadzu MPC 3100 spectrometer. Self-supported wafers of the samples were placed in a glass cell under vacuum. The samples were evacuated at 623 K and let stand under high vacuum overnight. Then they were exposed to pyridine vapors at room temperature for 30 min, followed by outgassing at 373 K. The concentration of the both types of acid sites was estimated assuming the extinction coefficients for the Brönsted and Lewis sites as 0.73 and 1.11 cm μmol^{-1}, respectively.

2.3. Catalytic studies

The oxidation of anthracene (see Fig. 1) was used as a model reaction in order to assess the catalytic activity of the synthesized catalysts. For the sake of comparison, the reaction was also conducted using a commercial zeolite Y (Si/Al = 1.5) as catalyst, which was kindly supplied by Degussa (Germany). Pore dimensions of this zeolite are close to the dimensions of some aromatic compounds, including the smaller PAHs, such as anthracene, and its acid strength is suitable for catalytic applications; in fact, this zeolite is the usual catalyst employed in fluid catalytic cracking of light naphtha streams.

Catalytic tests were performed at 348 K in a 100-mL three-necked round bottom flask, under mild stirring, by mixing 10 mL solvent, 160 mg anthracene, 100 mg catalyst and the required amount of oxidant (*t*-butylhydroperoxide, at a molar ratio of 8:1 with respect to anthracene) as described by Srinivas et al. [23], in order to avoid the non-selective thermal decomposition of the oxidant agent. The reacting mixture was allowed to stand in a silicon oil bath (348 K) for about 20 h, under magnetic stirring and reflux. The appearance of a brownish color, which is typical of quinones, was the first strong evidence of appreciable reaction conversion. Qualitative and quantitative chemical analysis of reactants and products was performed by liquid chromatography (HPLC) with UV/vis detector and/or by gas chromatography coupled with a mass spectrometry detector (GC/MS).

At the end of each reaction batch, the reacting mixture was allowed to cool at room temperature, after which it was dissolved in 5 mL of toluene and filtered. The spent catalyst was solvent extracted in a micro-reflux apparatus (4 h) and the liquor thus obtained was added to the initial filtrate. HPLC analysis was conducted in a Varian ProStar 150 chromatograph under isocratic mode, using CH_3CN–H_2O 80/20 (v/v) as mobile phase at a flow rate of 1 mL/min, analytical column C18 Chrom Spher 5 and the UV/vis detector set at $\lambda = 251$ nm. GC analysis was carried out in a Varian CP3800 chromatograph equipped with a flame ionization detector (FID) coupled to a mass spectrometer SATURN 2000 MS/MS. Analysis conditions were: capillary column CP-Sil 8.25 m × 0.25 mm (0.12 μm), H_2 as carrier gas, injector temperature of 523 K and FID temperature of 623 K.

3. Results and discussion

3.1. Synthesis and characterization of catalysts

Some modifications were introduced into the synthesis procedure described by Aguado et al. [25], such as a longer aging time of the solids in the synthesis liquor, the addition of a solvent extraction step and a shorter calcination time. These changes allowed the preparation of mesoporous materials with a high degree of isomorphic substitution and reduced occurrence of other crystalline structures (oxide and hydroxide phases) in the case of titanosilicates, which is evident from XPS results to be shown and discussed later. Reaction yields (on a dry basis) were over 40%, which may be considered as quite promising for this kind of methodology at room temperature. The fast hydrolysis of the Al and Ti alkoxides may lead to the ready formation of templated micelles in the acid phase [27] and thus reduced tetrahedral Al and Ti incorporated to the mesophase, Nevertheless, it seems that condensation in alkaline media was very efficient since high levels of heteroatom substitution were achieved in the synthesized mesoporous materials. ICP-OES elemental analysis confirms this observation, showing very good agreement between molar compositions in the synthesis gels and in the final solids (see Table 2).

3.1.1. XRD characterization

XRD powder patterns measured for the calcined (823 K) solids are shown in Fig. 2. In general, all samples show a distinct broad peak at $2.2^\circ < 2\theta < 3.2^\circ$, accounting for the Bragg plane (1 0 0), which is typical of the hexagonal structure of MCM-41 materials. Another characteristic peak of mesoporous MCM-41 materials may be observed at $4.2^\circ < 2\theta < 4.5^\circ$; for these samples, it is a rather flat peak, corresponding to the reflection (1 1 0). The absence of (2 0 0) and (2 1 0) Bragg planes indicates that there is a somewhat disordered hexagonal arrangement.

Calculated values for d_{100} and a_0 decreased for increasing amounts of incorporated Al and Ti, as reported by several other authors [8,28,29]. This behavior suggests a lower degree of crys-

Table 2
Physico-chemical characterization of MCM-41 and HMS calcined samples

Property	Sample			
	H-MCM-41	Al-MCM-41(10)	Ti-MCM-41(30)	Ti-HMS(30)
$(Si/metal)_{ICP-OES}$	∞	10	40	30
d_{100} (Å)	37.3	28.9	30.4	38.4
a_0 (Å)	43.1	33.4	35.2	44.3
BET surface area (m^2/g)	544.8	569.3	657.3	745.7
d_{pore} (Å)	41.4	32.4	31.1	28.1
V_{pore} (cm^3/g)	0.56	0.46	0.51	0.52
Acidity				
(mmol NH_3/g)	0.08	1.08	0.19	0.40
(μmol Py/g)	–	–	21.2	15.4

tallinity for mesoporous materials containing heteroatoms and may be associated to such factors as: (a) poor condensation of silanol groups in pore walls, (b) strong interaction between surfactant and heteroatom and (c) formation of micelles of reduced diameter [25].

3.1.2. Textural characterization

Fig. 3 shows adsorption/desorption N_2 isotherms at 77 K for the synthesized and calcined samples. In all cases, they are type IV isotherms, as classified by IUPAC [31]. Three distinct adsorption regions may be observed in the isotherms: the first one, $0.01 < P/P_0 < 0.42$, corresponds to the deposition of adsorbed layers on pore walls; the second one, $0.42 < P/P_0 < 0.80$, is related to capillary condensation of nitrogen in the pores (inflexion point between 0.35 and 0.40) and the third region, $P/P_0 > 0.80$, stands for multilayer adsorption on the external surface of the solid sample. No hysteresis is observed, which generally indicates the absence of other crystalline phases in the channels and a uniform filling of the mesopores with no hindrances to N_2 diffusion [32]. The surface areas of the catalysts (S_{BET}), as calculated from the BJH model, are relatively low for this type of materials (see Table 2). The inclusion of metals (Al and Ti) in the MCM-41 mesoporous structure caused a slight increase in surface area; on the other hand, pore diameter and pore volume decreased for increasing amount of incorporated metal. This is common behavior in this type of material since crystallinity reduces proportionally to the degree of isomorphic substitution of silicon. Moreover, unlike the hydrothermal route, the synthesis conditions thus employed do not favor the formation of regular channels within the solid matrix [33,34]. The main textural and physico-chemical properties of the synthesized samples are summarized in Table 2.

3.1.3. FTIR characterization

ATR-FTIR spectra obtained for four of the synthesized samples are extremely alike, mainly because the vibrations from symmetrical and asymmetrical stretching of Si–O–Si, Al–O–Si and Ti–O–Si bonds are detected in the same spectral region [35]. The broad band between 4000 and 3000 cm^{-1} is usually attributed to symmetrical and asymmetrical stretching vibrations of water bonded to the external surface (3400 cm^{-1}) and vibrations of OH group within the various silanol groups (isolated-SiOH at 3750 cm^{-1}, internal-SiOH at 3650 cm^{-1} or hydrogen bonded-SiOH at 3540 cm^{-1}). The band at 1630 cm^{-1} is commonly associated to the bending of H–O–H from adsorbed water, whereas the broad band between 1050 and 1250 cm^{-1}

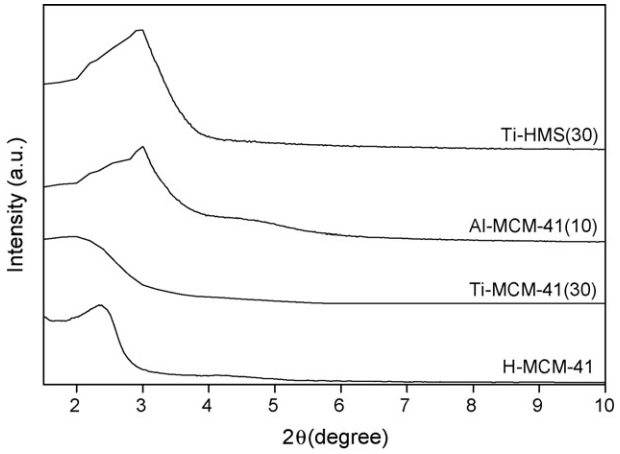

Fig. 2. XRD powder patterns for MCM-41, Al-MCM-41(10), Ti-MCM-41(30) and Ti-HMS(30) after being calcined at 823 K.

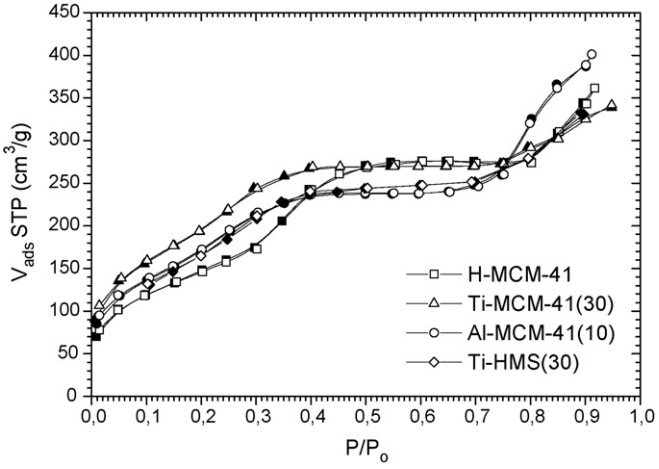

Fig. 3. N_2 adsorption isotherms at 77 K on samples of MCM-41, Al-MCM-41(10), Ti-MCM-41(30) and Ti-HMS(30) after calcination.

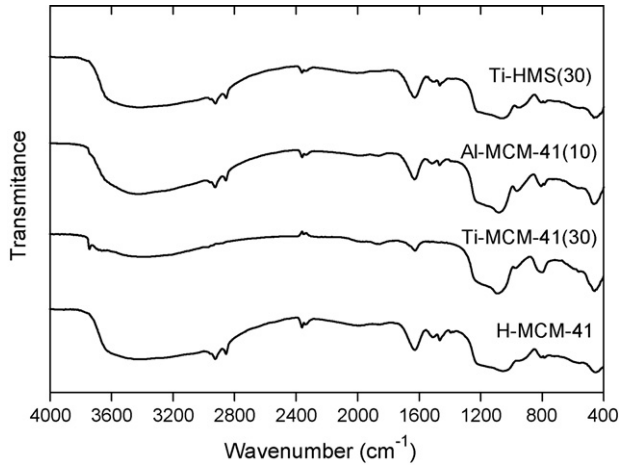

Fig. 4. ATR-FTIR spectra of the samples: MCM-41, Al-MCM-41(10), Ti-MCM-41(30) and Ti-HMS(30) after calcination.

refers to asymmetrical stretching of Si–O–Si within the mesoporous structure. In addition, the flat band at 970–962 cm^{-1} is good evidence of the incorporation of metallic heteroatoms to the purely siliceous MCM-41. This band is usually linked to stretching vibrations of –Si–O–Si– or –Si–O–M (M = Al, Zn, Ti, Zr, etc.) and its magnitude increases with the increasing amount of metal added to the structure due to superposition of bands [36]. The presence of bands at 3050–3120 cm^{-1} may be associated to the stretching of –C–H from the surfactant, showing that very stable structures are left even after calcination, which are capable of retaining templating molecules. The band at 800–820 cm^{-1} accounts for asymmetrical stretching in SiO_4 groups and its magnitude decreases for higher degrees of structural isomorphism as shown in Fig. 4.

3.1.4. Acidity characterization by TPD of ammonia and Py-FTIR

Total surface acidity may be estimated with this method for a relatively wide range of temperatures, since ammonia (a strong base) may interact with most acid sites both on the external surface and inside the pores of the sample. Fig. 5 shows the TPD-NH_3 curves (a) and the acidity histograms (b) for the calcined solids H-MCM-41, Al-MCM-41(10), Ti-MCM-41(30) and Ti-HMS(30).

The NH_3-TPD curves show a broad desorption band between 393 and 543 K, which suggests that there is a heterogeneous distribution of acid strength. Maximum desorption temperatures lied between 433 and 443 K, which evidences moderate to weak acid strength. It is clear that sample MCM-41 shows nearly no surface acidity, whereas sample Al-MCM-41(10) exhibits extremely acid properties (Table 2) and has the most heterogeneous acidity distribution of all studied samples. For the titanosilicates, the acidity of Ti-HMS(30) is considerably higher than that of sample Ti-MCM-41(30), probably due to the larger concentration of Brönsted and Lewis acid sites. In particular, acidity for such materials is related to the presence of isolated silanol groups (Si-OH), acid groups Al–OH, Ti–OH, Al–O–Si–OH and Ti–O–Si–OH and to electronically unbalanced structures containing Al and Ti ions. At temperatures above 773 K, there is still some amount of ammonia that has not been desorbed, which may be explained by the presence of some extremely strong acid sites in all samples.

The infrared spectra (Py-FTIR, not shown) of the samples indicate that there are both Brönsted and Lewis acid sites for all synthesized materials containing Al and Ti. Lewis acidity is lower for the Al-MCM-41(10) sample, for which nearly all of the acid sites may be assigned as Brönsted sites. On the other hand, the Ti-containing samples, Ti-MCM-41(30) and Ti-HMS(30),

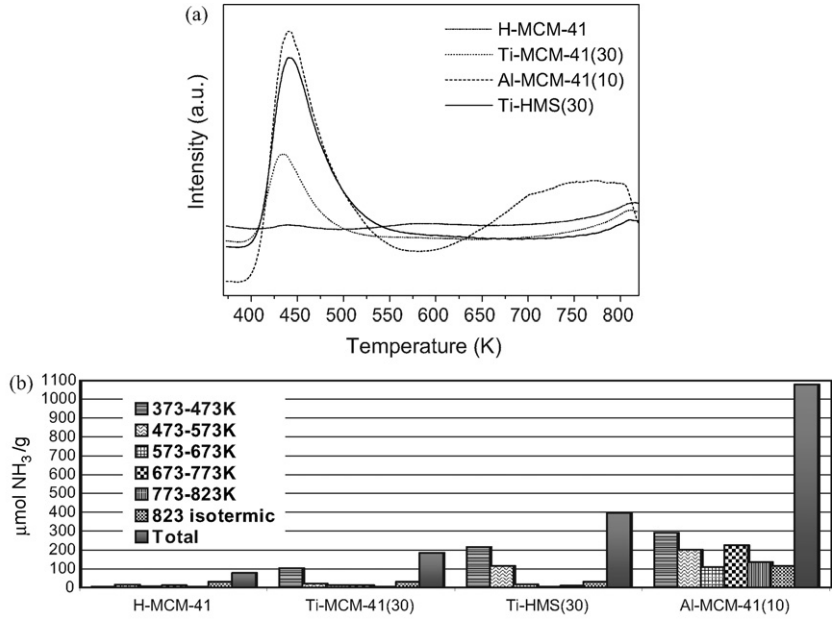

Fig. 5. Thermodesorption curves of ammonia (a) and acidity histograms (b) for the samples: MCM-41, Al-MCM-41(10), Ti-MCM-41(30) and Ti-HMS(30) after calcination.

show both Lewis and Brönsted sites. Lewis acidity values for these samples were found to be 15.4 and 21.1 μmol Py/g, respectively. Such concentration of Lewis acid sites seems to be enough to ensure the observed high catalytic activity for the experimental conditions under study.

3.1.5. XPS characterization

Selected XPS spectra of samples H-MCM-41, Ti-MCM-41(30) and Ti-HMS(30) are shown in Fig. 6. The core level O 1s spectrum in all studied samples shows an asymmetric signal, which can be decomposed into two peaks. The main peak, centered at 533.2 eV, is assigned to oxygen from silica. The absence of a contribution at low binding energy, at about 530.2eV, from TiO_2 or Al_2O_3, confirms the high isomorphic substitution for titanium and aluminum in Al-MCM-41 and Ti-MCM-41 samples. The other low intensity peak, which appears at a higher binding energy (about 534.0 eV) is assigned to surface silanol groups. For the titanosilicates, the core level Ti $2p_{3/2}$ signal at 460.0 eV is the same as that observed in titanosilicalite (TS-1) and is associated to tetrahedral Ti^{4+}. No peak was observed at 458.8 eV for the sample Ti-MCM-41, thus confirming the absence of TiO_2 [37–39]. These findings are consistent with regular dispersion of Ti^{4+} throughout the mesoporous matrix. For the sample Ti-HMS, a small shoulder at 458.1 eV indicates the possible formation of titanium oxide, and hence the presence of octahedrally coordinated Ti. The Si/Ti atomic ratio was estimated for the samples of titanosilicates. For Ti-HMS(30), this Si/Ti atomic ratio was found to be 28.6, which is very close to that found by ICP-OES. For Ti-MCM-41(30), however, the found Si/Ti atomic ratio was 89.5. This relatively low amount of Ti, as compared to the results from ICP-OES, suggests that titanium may be preferentially located in the interior of the solid and is more scarcely distributed at the solid surface. On the other hand, for sample Ti-HMS(30), titanium was evenly distributed both in the surface and in the interior of the solid. This fact had also been reported by Stakheef et al. [40] for low concentrations of this metal (lower than 5%) in the TiO_2–SiO_2 mixed oxide systems.

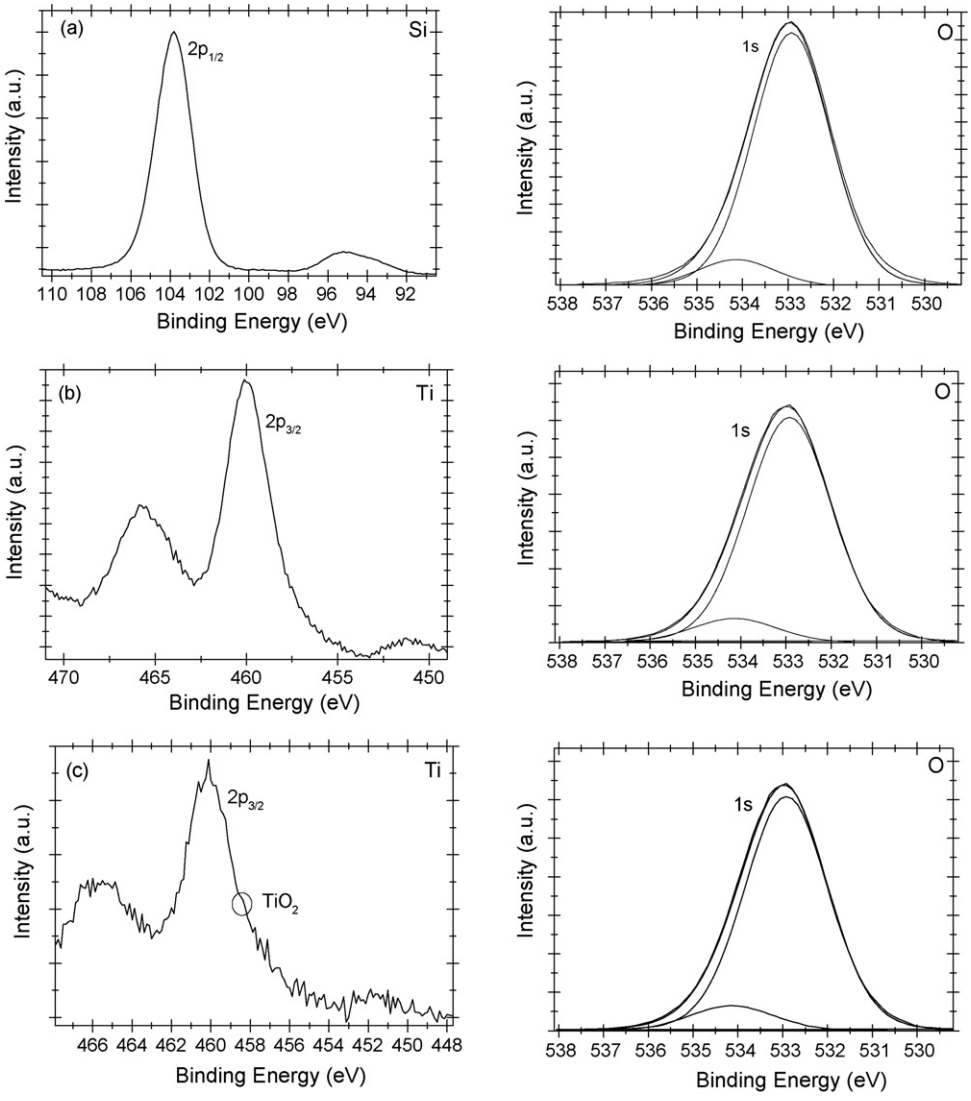

Fig. 6. XPS spectra of samples MCM-41(a), Ti-MCM-41(30) (b) and Ti-HMS(30) (c).

For the sample Al-MCM-41(10), the Si/Al molar ratio is 13.3, higher than that observed for the bulk, 10.3. This fact may be due to presence of Al inside the pores, non-detectable by XPS. The binding energy values for Si 2p (103.2 eV), and O 1 s (mean component at 532.5 eV, and a low intensity at 533.8 eV) are similar to those found for other mesoporous silica; and the observed value for Al 2p at 73.7 eV corresponds to the presence of Al^{3+}. It is well documented that the Al 2p binding energy does not give information to distinguish tetrahedral from octahedral Al [41,42], but it is possible to use the modified Auger parameter (α') to perform this distinction. In aluminosilicates, the Al α' values depends on the polarizability of the near neighbouring oxygen atoms, i.e. on the coordination. Thus, α' values higher than 1461.0 eV are characteristic of octahedral Al, whereas tetrahedral Al exhibits α' values lower than 1460.4 eV. In Fig. 7, the Al KLL spectra for sample Al-MCM-41(10) and for a commercial γ-Al_2O_3 are shown. The Al KLL spectrum of sample Al-MCM-41(10) shows two peaks, but with different intensities; a low intensity one with a α' value of 1459.1 eV assigned to framework tetrahedral Al, and a high intensity one with an α' of 1461.3 eV, very similar to that observed in the case of γ-Al_2O_3. It is clear that there is an excess of Al as Al_2O_3 on the surface. This fact can explain the lower observed surface area of sample Al-MCM-41(10) in comparison with the titanium-containing silica due to the presence of surface Al_2O_3 blocking some of the pores. The sample MCM-41 shows the Si 2p signal centered at about 104.0 eV, assigned to Si from silica.

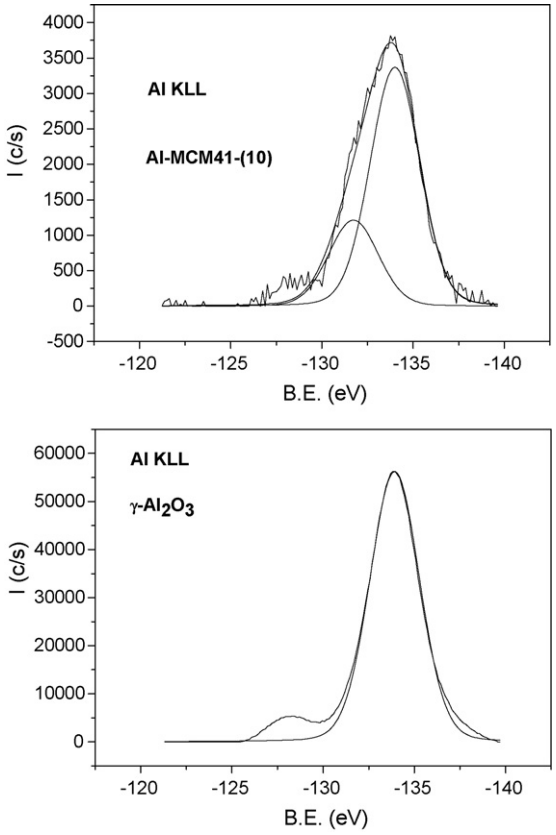

Fig. 7. Al_{KLL} Auger signal for samples γ-Al_2O_3 and Al-MCM-41(10).

Table 3
Conversions and selectivities for 9,10-anthraquinone measured for the reaction of anthracene in liquid phase at 348 K catalyzed by the synthesized materials and Y zeolite

Catalyst	Conversion of anthracene (%)	Selectivity for 9,10-anthraquinone (%)	Others (%)
H-MCM-41	9.6	31.3	68.7
Al-MCM-41(10)	92.4	23.2	76.8
Ti-MCM-41(30)	71.2	72.5	27.5
Ti-HMS(30)	93.9	96.8	3.2
Y zeolite	33.3	28.3	71.7
None	2.2	0.9	–

3.2. Catalytic (redox) activity on MCM-41 and HMS materials

Table 3 summarizes the results for conversion and selectivity obtained for the oxidation of anthracene with *tert*-butylhydroperoxide using the synthesized materials as catalysts. The data show high conversions for materials Al-MCM-41(10), Ti-MCM-41(30) and Ti-HMS(30), low conversion for zeolite Y and a very low conversion of 9.6% for the purely siliceous material (MCM-41) with a selectivity to 9,10-anthraquinone of 31.3%. These values are very similar to those observed by Srinivas et al. [23] with a pure MCM-41 operating at 353 K. In the absence of catalyst, no appreciable hydroxylation of anthracene was observed and only traces of the target product, 9,10-anthraquinone, were formed.

Higher yields for the target product, 9,10-anthraquinone, were obtained for Ti-MCM-41(30) and Ti-HMS(30) (51.6 and 90.9%, respectively), which have a considerable density of acid sites of moderate strength. The observed yield in the case of sample Ti-HMS(30) is very high and close to the highest value reported in literature, with Cr-MCM-41 [23]. However, Srinivas et al. [23] reported a very low conversion of anthracene (∼5%) for a Ti-MCM-41 (∼1 wt%) sample with a selectivity towards the quinone of nearly 35%. The different synthesis procedure and the distinct content of Ti may be the reasons for the observed discrepancy in the catalytic performance with the Ti-containing samples. Ti-MCM-41(30) and Ti-HMS(30) samples contain 3.4 and 3.5 wt% of Ti, a much higher content than that of sample Ti-MCM-41 (∼1 wt%) prepared by Srinivas et al. [23]. The acidity of our Ti-containing sample must be also higher if the Ti content is considered, but unfortunately, Srinivas et al. [23] did not report the acidity of their solids for comparison. The better catalytic performance of sample Ti-HMS(30) as compared to sample Ti-MCM41(30) can be explained by taking into account its higher surface area and acidity. The higher acidity of sample Ti-HMS(30) may be a direct consequence of the lower Si/Ti molar ratio on the surface, as indicated by the XPS results. For the sample Al-MCM-41(10), a high conversion is obtained at the expense of low selectivity for 9,10-anthraquinone, which shows the adverse effect of the high concentration of Brönsted acid sites in this kind of reaction. According to Zhang et al. [43], Brönsted acid sites from silanol groups, isolated aluminum and bridging hydroxyl groups attributed to isomorphic aluminum in pore walls are the main

sources of active catalytic sites for the hydroxylation of benzene and other aromatics.

The lower values for both anthracene conversion and selectivity for 9,10-anthraquinone obtained with zeolite Y (d_p = 7.4 Å) may be explained by the diffusional limitations and to adverse shape selectivity for the chemical species involved in the reaction. On the other hand, for the mesoporous titanates Ti-MCM-41 (d_p = 31.1 Å) and Ti-HMS (d_p = 28.1 Å), the relatively large pores and the polar nature of acid sites favor surface selectivity towards polar molecules or those with a higher aromatic polarizability, which enhances the adsorption of such molecules and subsequent reaction steps. The molecule of anthracene, which is rich in π-electrons, should be most likely attracted to the catalyst surface by means of electrostatic interactions with Brönsted acid sites, followed by the chemical conversion to 9,10-anthraquinone by means of Lewis acid sites. This hypothesis is consistent with the reaction parameters obtained for Al-MCM-41(10), which have practically only Brönsted acid sites. In such case, adsorption and catalysis take place mainly by means of hydroxyl groups and hence hydroxylation of the aromatic ring is the predominant reaction. The high concentration of hydroxylated products, detected by GC/MS, confirms this assumption. In general, the presence of Ti outside the mesoporous framework (TiO_2) and under other coordination states had little effect on the catalytic activity of the studied materials.

For the sample Ti-HMS, the catalyst with the best performance in the model-reaction, further kinetic studies were conducted at 320, 335 and 348 K. Fig. 8 shows reaction conversion as a function of time and it is clear that this parameter is quite affected by temperature variations.

At 320 K, the reaction practically does not occur (maximum conversion = 34.7%). On the other hand, a raise in temperature to 335 and 348 K increases conversion to 55 and 95%, respectively. At 348 K, conversions over 80% were reached within the first 10 h of reaction. The assumption of a pseudo-first-order rate law for the oxidation reaction led to rate constants (k) of 2.12×10^{-2}, 3.97×10^{-2} and $13.91 \times 10^{-2}\,h^{-1}$, for temperatures of 320, 335 and 348 K, respectively. The activation energy was calculated according to the Arrhenius law and it was found to be approximately 15.2 kcal/mol. Smith and Notheisz [44] state that values of this order of magnitude evidence kinetic control by reaction phenomena on the catalyst surface. Values lower than 5 kcal/mol are characteristic of reactions controlled by diffusion in the fluid phase.

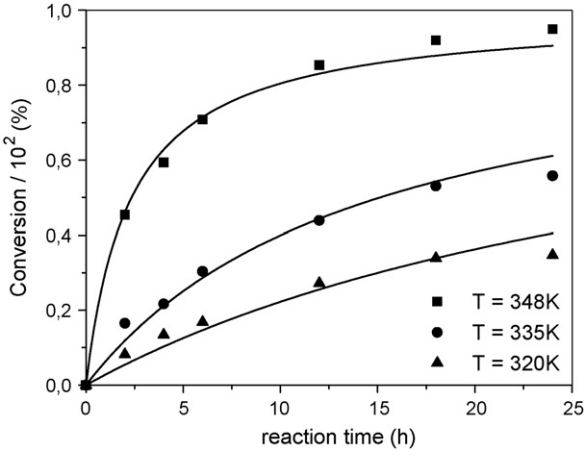

Fig. 8. Effect of temperature on the oxidation reaction of anthracene over catalyst Ti-HMS(30). C_0: 90 mmols/L, mass of catalyst: 80 mg, 10 mL benzene, molar ratio t-BHP/anthracene = 50, total reaction time = 24 h.

Table 4
Experimental domain of studied variables in the reaction of oxidation of anthracene over mesoporous catalyst Ti-HMS(30)

Type of design	Coded factors (levels)	Actual values	
		ROA	Q_{cat} (g/L)
Factorial	−1.0	3.0	2.0
	+1.0	8.0	5.0
Center point	0.0	5.5	3.5
Rotatable	−1.4	2.0	1.4
	+1.4	9.0	5.6

In addition, modeling and optimization of the oxidation reaction at 348 K using the Ti-HMS sample was performed by means of factorial design [45] for the variables oxidant/anthracene molar ratio (ROA) and amount of catalyst (Q_{cat}). Table 4 shows the experimental domain associated to the dependent and independent variables under study in the oxidation reaction of anthracene. Eleven experiments were designed (including three replicates at the central point) and performed according to this design, which are shown in Table 5. For these experiments, initial concentration of polyaromatic was 90 mmols/L, benzene was used as solvent (10 mL) and *tert*-butylhydroperoxide as oxidant, at 348 K with a reaction time of 24 h. Independent variables were oxidant/anthracene molar ratio (ROA = x_1) and amount of catalyst ($Q_{cat} = x_2$). Dependent variables or experimental responses were chosen as percent anthracene conversion (Y_1) and percent 9,10-anthraquinone yield (Y_2). Table 5 also includes the results of Y_1 and Y_2 obtained for each of the performed experiments. The generic model used to correlate x_1 and x_2 to each of the studied experimental responses is expressed by

Table 5
Experimental matrix and respective experimental responses for the oxidation reaction of anthracene over mesoporous catalyst Ti-HMS(30) at 348 K

Experiment	Variables		Response averages	
	x_1	x_2	Y_1 (%)	Y_2 (%)
01	−1.000	−1.000	66.18	77.72
02	−1.000	1.000	78.37	95.12
03	1.000	−1.000	84.82	80.84
04	1.000	1.000	86.81	93.32
05	−1.414	0.000	60.55	90.13
06	1.414	0.000	85.52	85.85
07	0.000	−1.414	66.69	73.33
08	0.000	1.414	87.26	90.55
09	0.000	0.000	90.01	96.88
10	0.000	0.000	88.12	94.04
11	0.000	0.000	89.89	94.99

Y_1, experimental response for percent conversion (average from duplicates); Y_2, experimental response for percent selectivity (average from duplicates).

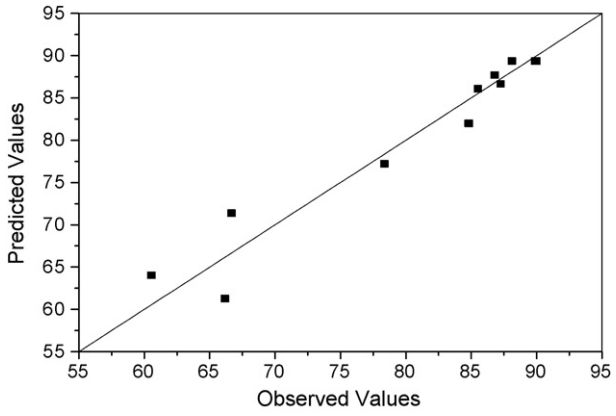

Fig. 9. Values predicted by model Eq. (3) as compared to experimentally measured values for the percent conversion of the reaction of oxidation of anthracene in liquid phase at 348 K.

Eq. (2).

$$Y = b_0 + b_1x_1 + b_2x_2 + b_{11}x_1^2 + b_2x_2^2 + b_{12}x_1x_2 \quad (2)$$

where b_0 represents the model independent term and b_{ij} are the model coefficients to be determined by regression procedures. For the set of 11 experiments performed, the best regression for percent conversion and percent selectivity, respectively, is expressed by Eqs. (3) and (4). Cross-interaction between the two studied independent variables (term $b_{12}x_1x_2$) was found to be negligible in both cases.

$$Y_1 = 89.34 + 8.549x_1 + 6.159x_2 - 6.767x_1^2 - 4.797x_2^2 \quad (3)$$

$$Y_2 = 94.637 + 7.154x_2 - 2.689x_1^2 - 5.714x_2^2 \quad (4)$$

In general, the regression expressions (Eqs. (3) and (4)) satisfactorily represent the relations between dependent and independent variables under study. Correlation coefficients for the responses percent conversion (Y_1) and percent selectivity (Y_2) were found to be 0.9418 and 0.9616, respectively. In Figs. 9 and 10, obtained experimental values are compared to those calculated from the model equations for conversion and selectivity, respectively.

For the range of the variables under study, ROA between 3 and 8 and amount of catalyst (Q_{cat}) between 20 and 100 mg, the statistical analysis employed indicated optimal molar ratio of 5.5 (oxidant/aromatic ratio) and a mass of catalyst of 44.3 mg, both leading to anthracene conversion and selectivity for 9,10-anthraquinone higher than 91%.

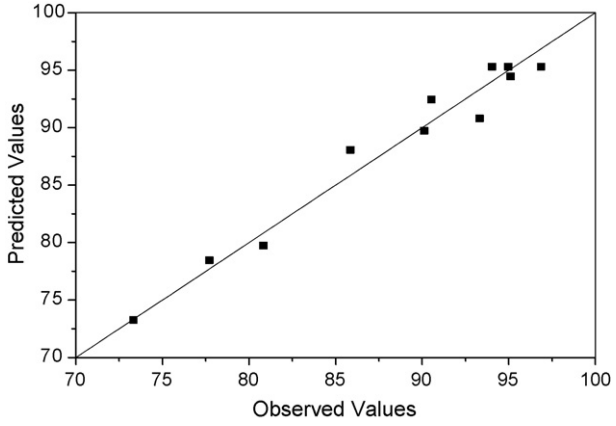

Fig. 10. Values predicted by model Eq. (4) as compared to experimentally measured values for the percent selectivity towards 9,10-anthraquinone in the reaction of oxidation of anthracene in liquid phase at 348 K.

4. Conclusions

Mesoporous sílica of MCM-41 type containing heteroatoms such as Ti or Al are very active catalysts in the oxidation of anthracene in liquid phase at 348 K, using benzene as solvent and *tert*-butylhydroperoxide as oxidant agent. The conversion of anthracene and the selectivity to 9,10-anthraquinone are very affected by the nature and concentration of the surface acid sites. When the Brönsted acidity is very high, sample Al-MCM-41(10), a low selectivity to 9,10-anthraquinone, and a high proportion of secondary hydroxylated products are observed. In the case of sample Ti-HMS, an excellent catalytic performance is observed with a conversion of anthracene and selectivity to 9,10-anthraquinone higher than 90%. This may be due to a balanced distribution of Brönsted and Lewis acid sites, which should be further investigated in future work. These non-containing toxic ion metal catalysts merit for separation processes or in heterogeneous catalysis of bulky aromatics from liquid organic streams.

Acknowledgements

The authors wish to thank CAPES (collaboration Brazil/Spain, project 84/05), Spanish MECD project HBP2004-0020, the National Petroleum Agency (ANP) and FUNCAP (Fundação Cearense de Apoio ao Desenvolvimento Científico e Tecnológico) for the financial support granted to this work. Support from Prof. Dulce Melo (Universidade Federal do Rio Grande do Norte, Brazil) with BET analyses is gratefully acknowledged.

References

[1] J.S. Beck, J.C. Vartuli, W.J. Roth, M.E. Leonowicz, C.T. Kresge, K.D. Schmitt, C.T.-W. Chu, D.H. Olson, E.W. Sheppard, S.B. McCullen, J.B. Higgins, J.L. Schlenker, J. Am. Chem. Soc. 114 (1992) 10834.
[2] C.T. Kresge, W.J. Leonowicz, J.C. Roth, J.C. Vartulli, J.S. Beck, Nature 359 (1992) 710.
[3] M.L. Occelli, S.J. Biz, J. Mol. Catal. A 151 (2000) 225.
[4] B. Lindlar, A. Kogelbauer, P.J. Kooyman, R. Prins, Microporous Mesoporous Mater. 89 (2001) 44.
[5] M.E. Davis, C.Y. Chen, S.L. Burket, H.X. Li, Microporous Mater. 2 (1993) 17.
[6] M.L. Occelli, S.J. Biz, Catal. Rev. Sci. Eng. 40 (3) (1998) 329.
[7] P. Selvam, S. Badamali, A. Sakthivel, Catal. Today 63 (2000) 291.
[8] L.Y. Chen, Z. Ping, G.K. Chuah, S. Jaenicke, G. Simon, Microporous Mesoporous Mater. 27 (1999) 231.
[9] M. Ziolek, Catal. Today 90 (2004) 145.
[10] W. Adam, C.M. Mitchell, C.R. Sacha-Möller, T. Selvam, O.J. Weichold, J. Mol. Catal. A 154 (2000) 251.

[11] A. Corma, M.S. Grande, V. Gonzalez-Alfaro, A.V. Orchilles, J. Catal. 159 (1996) 375.
[12] W. Reschetilowski, H. Koch, Microporous Mesoporous Mater. 25 (1998) 127.
[13] G. Seo, N.H. Kim, Y.H. Lee, J.H. Kim, Catal. Lett. 90 (2004) 145.
[14] M.V. Landau, E. Dafa, M.L. Kaliya, T. Sen, M. Herskowitz, Microporous Mesoporous Mater. 49 (2001) 65.
[15] Y. Ohtsuka, Y. Takahashi, M. Noguchi, A. Takashi, S. Takasaki, N. Tsubouchi, Y. Wang, Catal. Today 89 (2004) 419.
[16] T. Klimova, M. Calderon, J. Ramírez, Appl. Catal. A 204 (2003) 29.
[17] S. Gontier, A. Tuel, J. Catal. 157 (1996) 124.
[18] M. Yonemitsu, Y. Tanaka, M. Iwamoto, J. Catal. 178 (1998) 207.
[19] Q. Zhang, Y. Wang, Y. Ohishi, T. Shishido, K. Takehira, J. Catal. 202 (2001) 308.
[20] L. Noreña-Franco, I. Hernandez-Perez, A. Aguilar-Pliego, A. Maubert-Franco, Catal. Today 75 (2002) 189.
[21] B.L. Su, C. Constantin, V. Pârvulescu, J. Mol. Catal. A 202 (2003) 171.
[22] N. Srinivas, V. Radha Rani, S.J. Kulkarni, M. Radha kishan, K.V. Raghavan, J. Mol. Catal. A 172 (2001) 187.
[23] N. Srinivas, V. Radha Rani, S.J. Kulkarni, K.V. Raghavan, J. Mol. Catal. A 179 (2002) 221.
[24] R.H. Chung, Kirh-Othmer Encyclopedia of Chemical Technology, vol. 2, John Wiley and Sons, New York, 1985, p. 700.
[25] J. Aguado, D.P. Serrano, J.M. Escola, Microporous Mesoporous Mater. 34 (2000) 43.
[26] Y. Luo, G.Z. Lu, Y.L. Guo, Y.S. Wang, Catal. Commun. 3 (2002) 129.
[27] T. Blasco, A. Corma, M.T. Navarro, J. Pérez-Pariente, J. Catal. 156 (1995) 65.
[28] W. Zhang, M. Froba, J. Wang, J. Wong, P.T. Tanev, T.J. Pinnavaia, J. Am. Chem. Soc. 118 (1996) 9164.
[29] A. Corma, V. Fornés, M.T. Navarro, J. Pérez-Pariente, J. Catal. 148 (1994) 569.
[31] K. Sing, J. Rouquérol, F. Rouquérol, Adsorption by Powders and Porous Solids: Principles, Methodology and Applications, Academic Press, London, 1990.
[32] T.P. Tanev, L.T. Vlaev, J. Colloid Interface Sci. 160 (1993) 110.
[33] A. Sayari, Stud. Surf. Sci. Catal. 102 (1996) 1.
[34] A. Sayari, M. Kruk, M. Jaroniec, Microporous Mesoporous Mater. 27 (1999) 217.
[35] V.L. Zholobenko, S.M. Holmes, C.S. Cundy, J. Dwyer, Microporous Mater. 11 (1997) 83.
[36] L. Chen, S. Jaenicke, G.K. Chuah, Microporous Mater. 12 (1997) 323.
[37] A. Tuel, Microporous Mesoporous Mater. 27 (1) (1999) 51.
[38] S. Klein, B.M. Weckhuysen, J.A. Martens, W.F. Maier, P.A. Jacobs, J. Catal. 163 (1996) 489.
[39] N. Lang, P. Delichere, A. Tuel, Microporous Mesoporous Mater. 56 (2002) 203.
[40] A.Y. Stakheef, E.S. Shpiro, J. Apijok, J. Phys. Chem. 97 (1993) 5668.
[41] M.J. Remy, M.J. Genet, G. Pocelet, P.F. Lardinois, P.P. Nottè, J. Phys. Chem. 96 (1992) 2614.
[42] J.M. Mérdia-Robles, P. Olivera-Pastor, A. Olivera-Pastor, A. Jiménez-López, E. Rodríguez-Castellón, J. Phys. Chem. 100 (1996) 14726.
[43] W. Zhang, J. Wang, P.T. Tanev, T. Pinnavaia, Chem. Commun. (1996) 979.
[44] G.V. Smith, F. Notheisz, Heterogeneous Catalysis in Organic Chemistry, Academic Press, San Diego, 1999.
[45] G.E.P. Box, W.G. Hunter, J.S. Hunter, Statistic for Experimenters. An Introduction to Design, Data Analysis and Model Building, John Wiley and Sons, New York, 1978.

Further reading

[30] A. Matsumoto, H. Chen, K. Tsutsumi, M. Grun, Microporous Mesoporous Mater. 32 (1999) 55.